

Supporting Information

Multifaceted Luminescence in Lanthanide-Activated Microrods for Advanced Multicolor Anti-Counterfeiting

Qianyu Zheng[†], Lili Xie^{†,*}

Department of Health Inspection and Quarantine, School of Public Health, Fujian Medical University, Fuzhou, 350122, Fujian, China

**Correspondence: Lili Xie, 1006xielili@fjmu.edu.cn*

†These authors have contributed equally to this work.

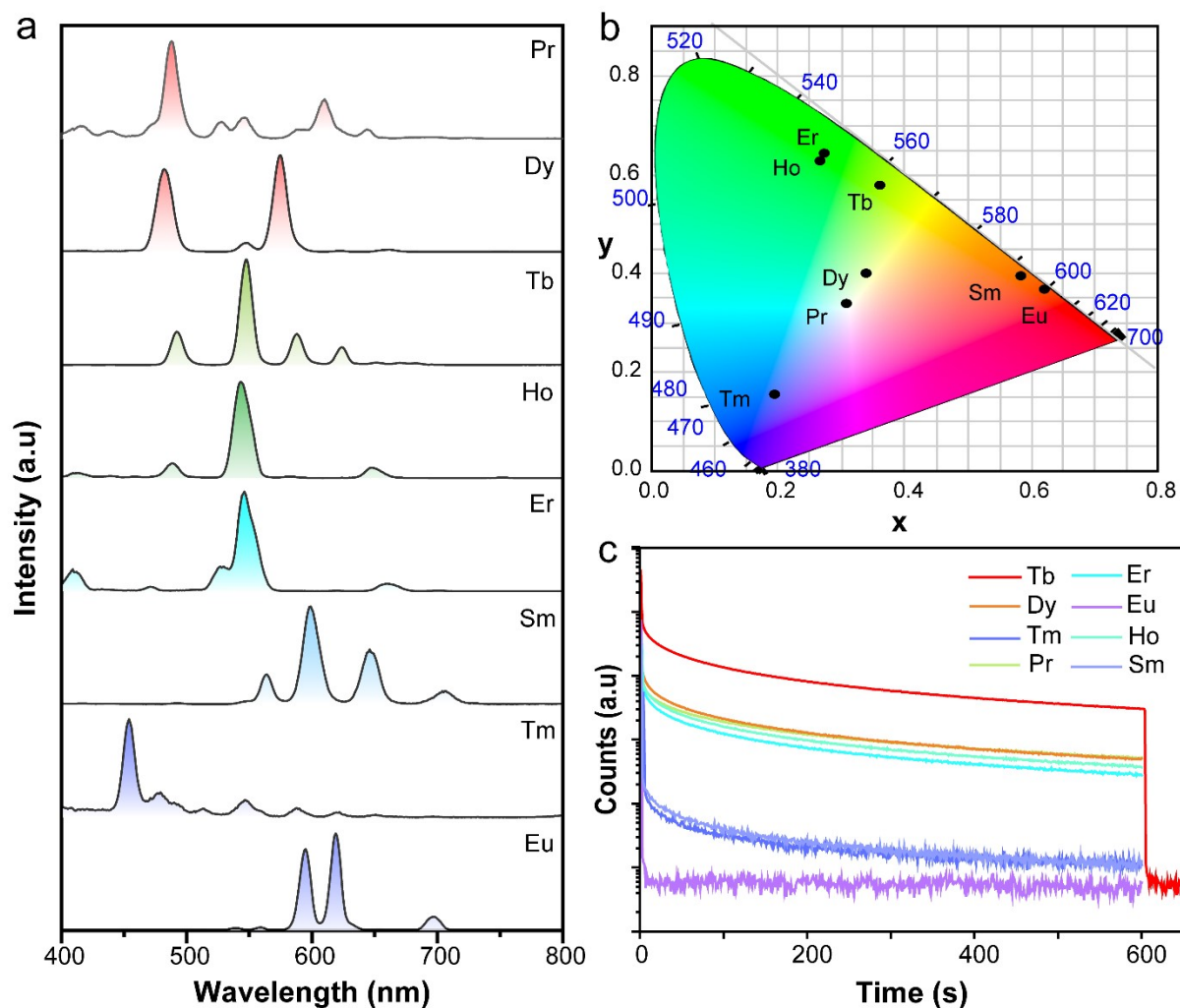


Figure S1. Characterization of persistent luminescence microrods doped with different lanthanide activators. (a) Room-temperature X-ray luminescence spectra of $\text{NaYF}_4:\text{Ln}^{3+}$ ($\text{Ln}^{3+}=\text{Pr}^{3+}, \text{Dy}^{3+}, \text{Tb}^{3+}, \text{Ho}^{3+}, \text{Er}^{3+}, \text{Sm}^{3+}, \text{Tm}^{3+}, \text{Eu}^{3+}$) microrods. (b) Corresponding Commission Internationale de l'Éclairage (CIE) chromaticity Diagram of persistent luminescence. (c) Room-temperature afterglow decay curves of $\text{NaYF}_4:\text{Ln}^{3+}$ ($\text{Ln}^{3+}=\text{Pr}^{3+}, \text{Dy}^{3+}, \text{Tb}^{3+}, \text{Ho}^{3+}, \text{Er}^{3+}, \text{Sm}^{3+}, \text{Tm}^{3+}, \text{Eu}^{3+}$) microrods monitored at 488 nm, 575 nm, 546 nm, 544 nm, 546 nm, 599 nm, 479 nm, and 618 nm, respectively. Dose rate, $278 \mu\text{Gy s}^{-1}$; excitation time, 180 s.

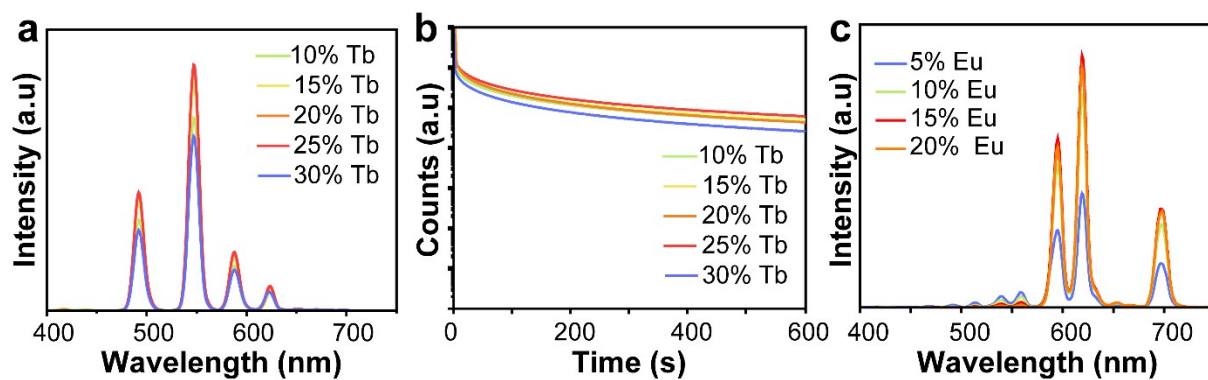


Figure S2. X-ray luminescence spectra (a) and afterglow spectra (b) of NaYF₄:xTb³⁺ microrods doped with different Tb³⁺ contents, (x=10-30 mol%). (c) X-ray luminescence spectra of NaYF₄:xEu³⁺ microrods doped with different Eu³⁺ contents, (x=5-20 mol%).

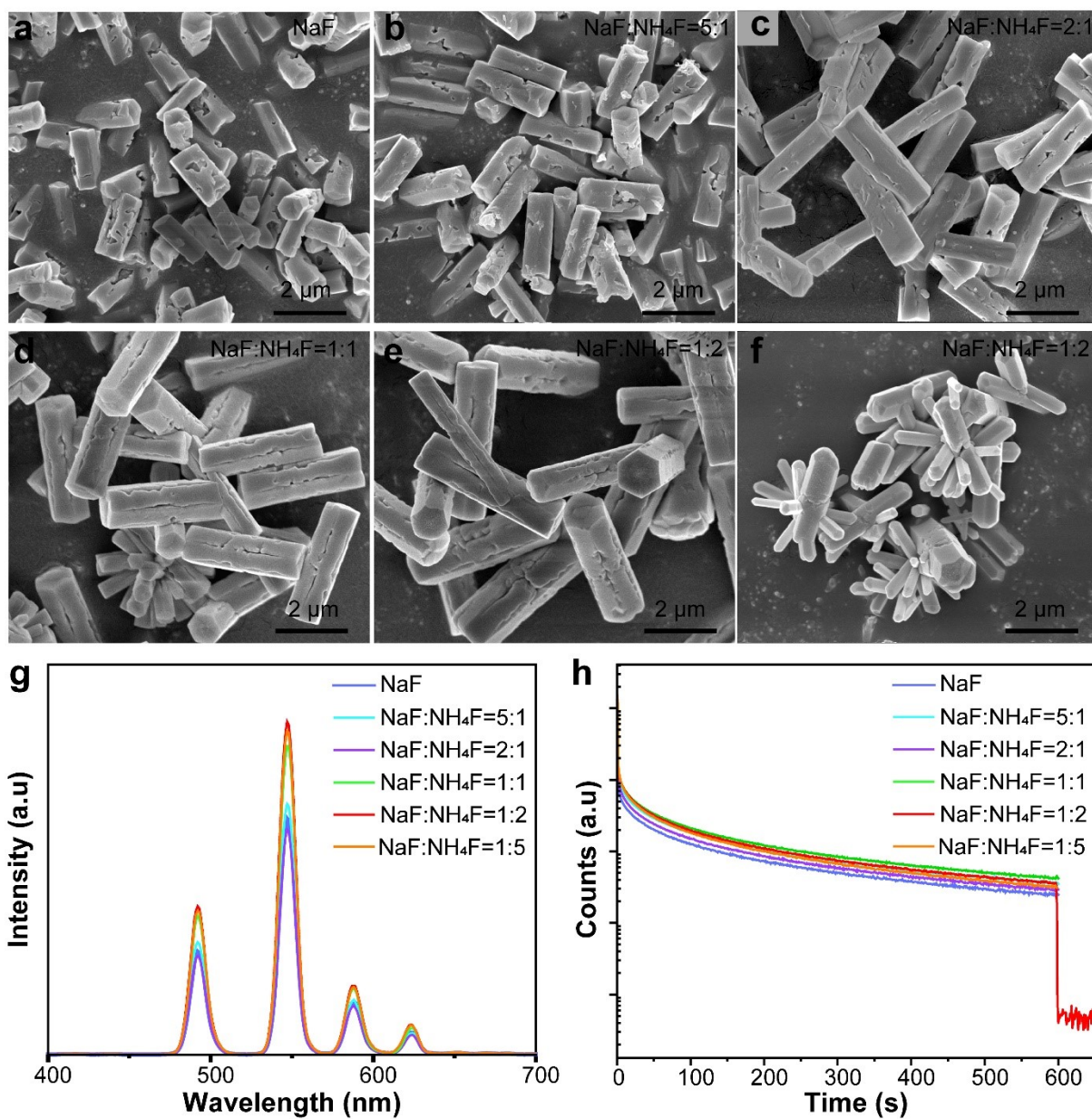


Figure S3. Crystal morphology modulated by F ions. Scanning electron micrographs (a), X-ray luminescence spectra (b), and afterglow spectra (c) of NaYF₄:Tb³⁺ prepared with different ratios of NaF and NH₄F.

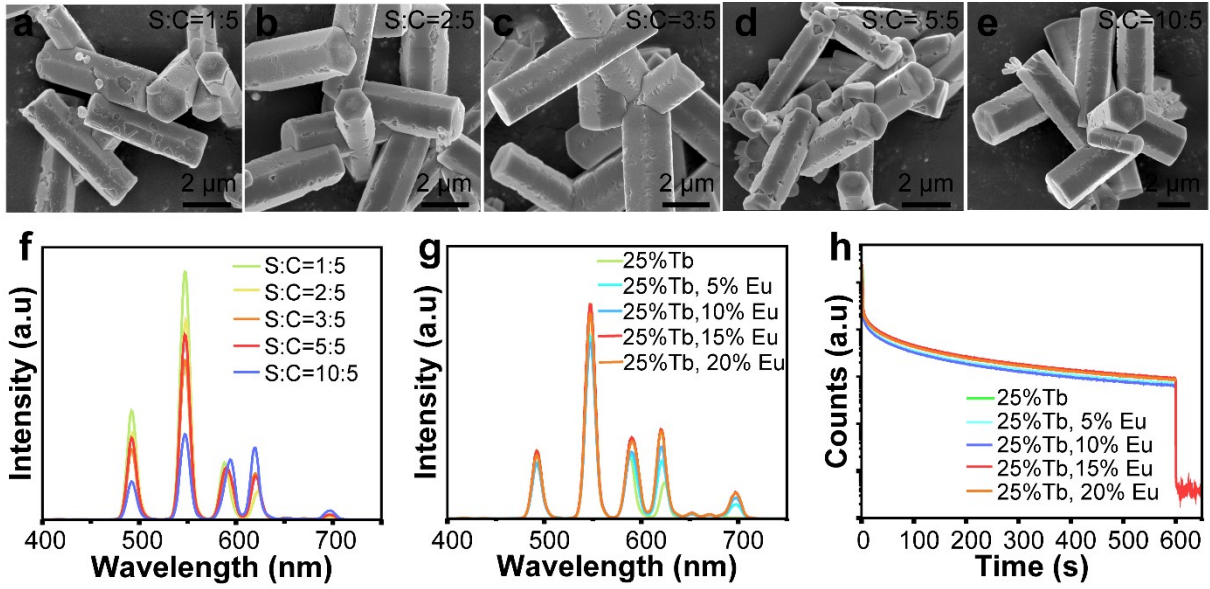


Figure S4. SEM images of microrods grown with various ratios of shell precursor solution (a-e) and the corresponding X-ray luminescence spectra (f). X-ray luminescence spectra (g) and afterglow luminescence spectra (h) of microrods generated by doping various activator concentrations with the same molar shell layer precursor liquid. S:C represents the epitaxial growth precursor to core molar ratio.

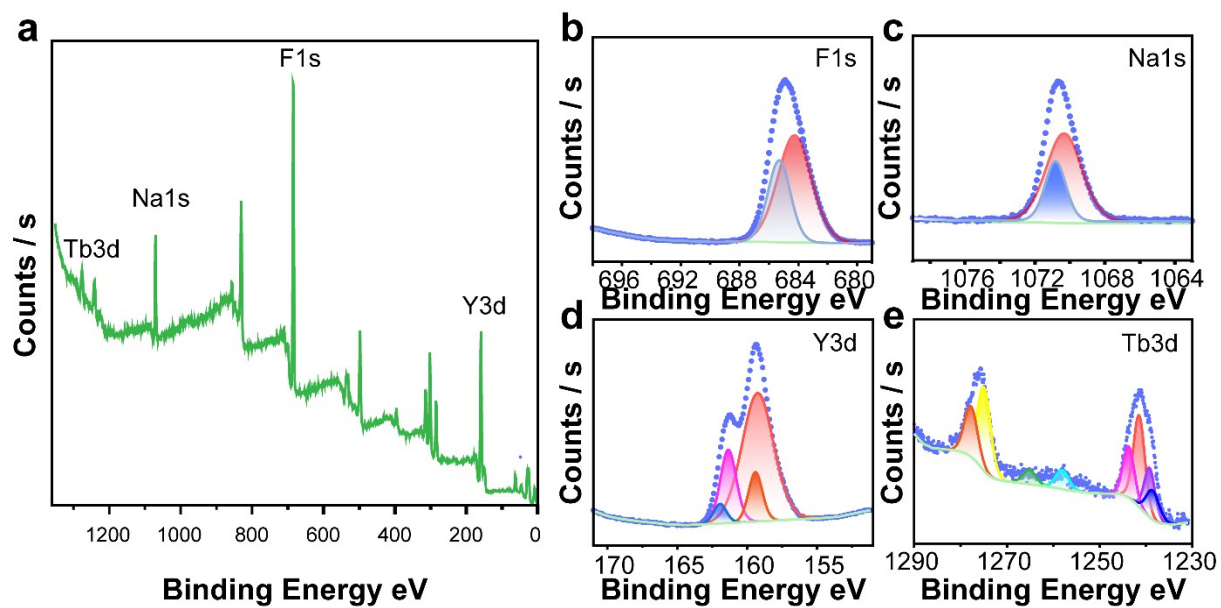


Figure S5. (a) XPS survey spectrum of NaYF₄:Tb³⁺(25 mol%) microrods. High resolution spectra of (b) F, (c) Na, (d) Y, and (e) Tb.

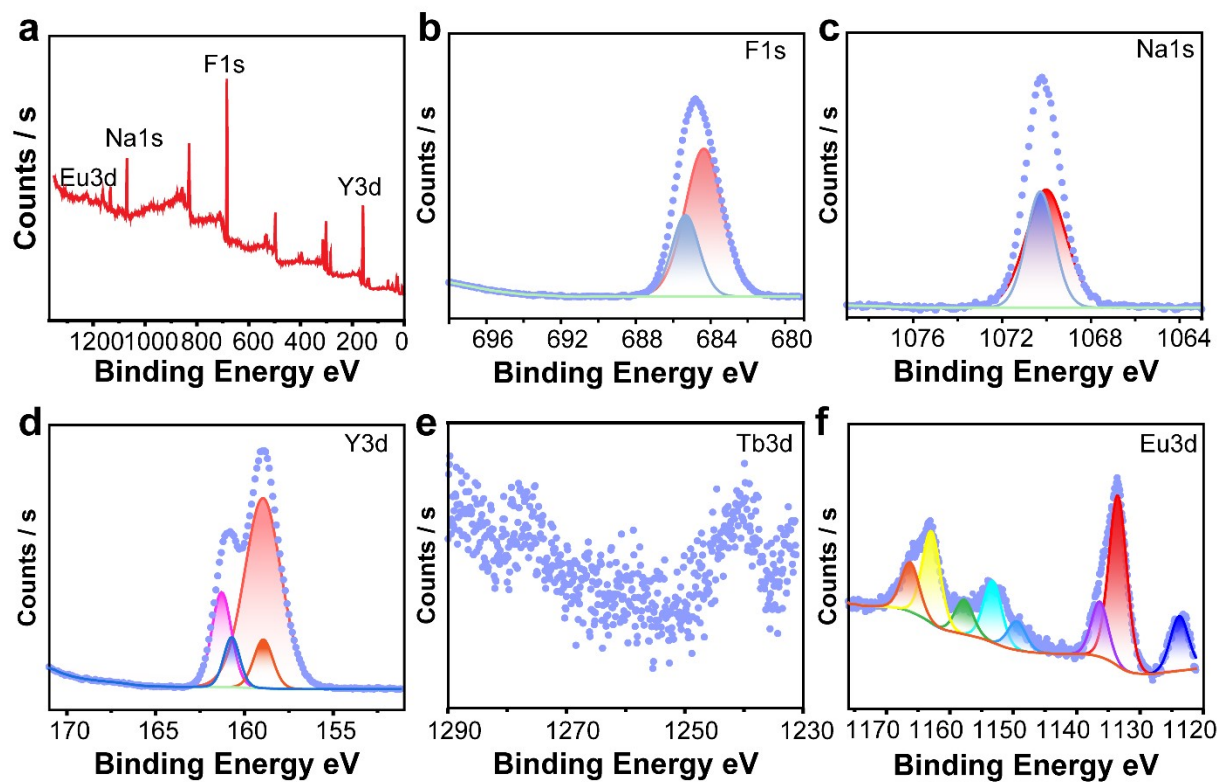


Figure S6. (a) XPS survey spectrum of NaYF₄:Tb³⁺(25 mol%)/NaYF₄:Eu³⁺(15 mol%) microrods. High resolution spectra of (b) F, (c) Na, (d) Y, (e) Tb, and (f) Eu.

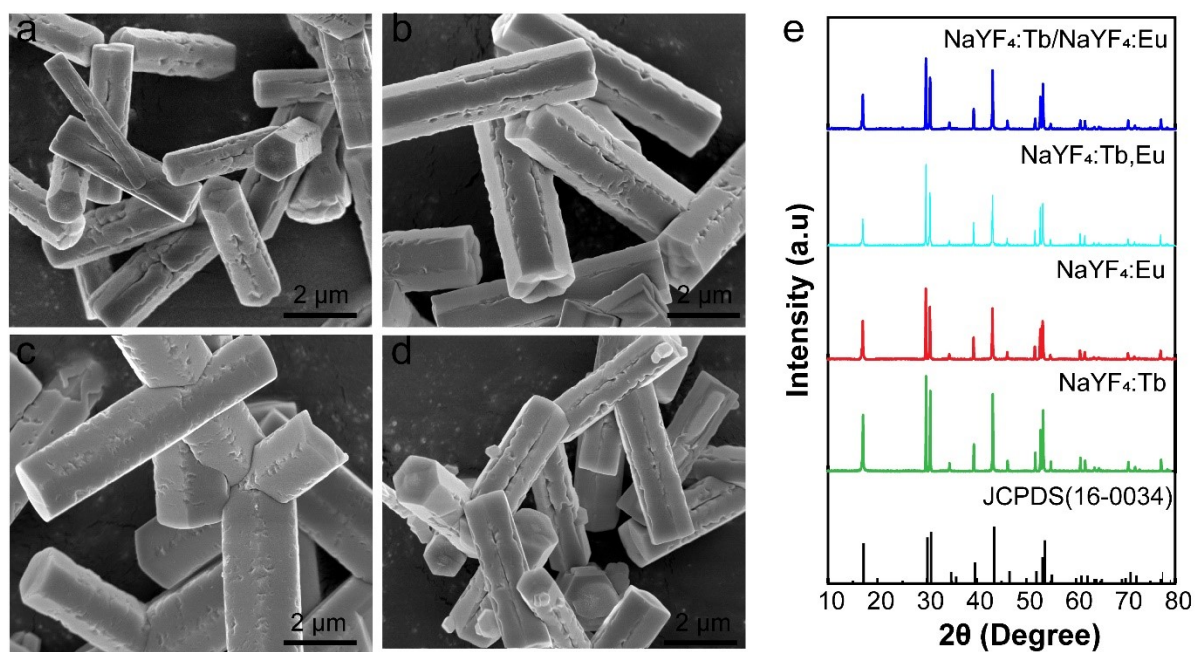


Figure S7. SEM images of (a) NaYF₄:Tb³⁺ (25 mol%), (b) NaYF₄:Eu³⁺ (15 mol%), (c) NaYF₄:Tb³⁺(25 mol%)/NaYF₄:Eu³⁺ (15 mol%), (d) NaYF₄:Tb³⁺, Eu³⁺ (25, 0.5 mol%), and the corresponding X-ray powder diffraction spectrum (e).

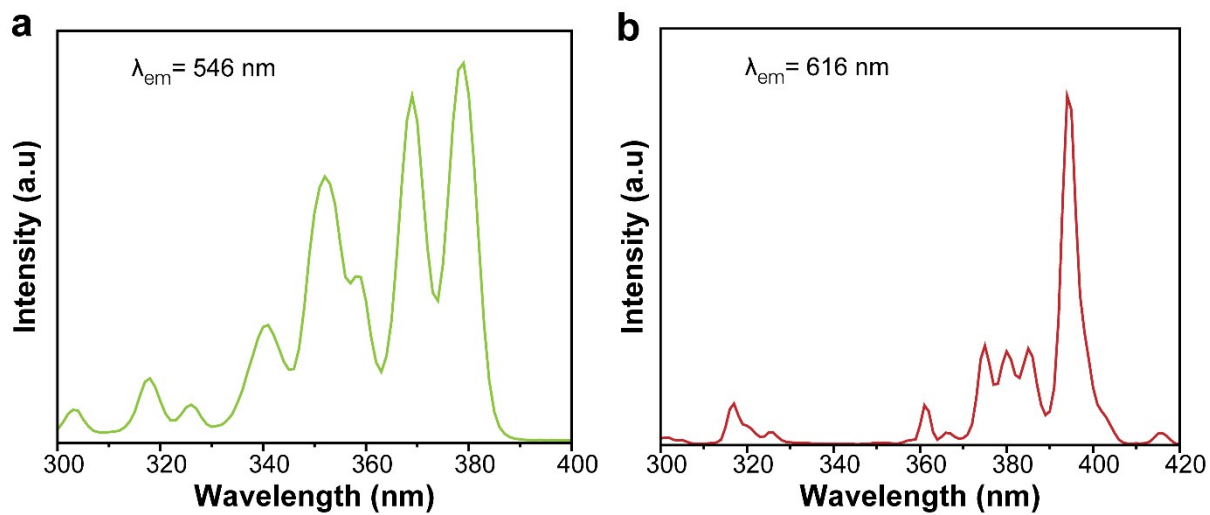


Figure S8. Excitation spectra of NaYF₄:Tb³⁺(25 mol%)/NaYF₄:Eu³⁺(15 mol%). The detection wavelengths were Tb³⁺ 546 nm (a) and Eu³⁺ 616 nm (b).

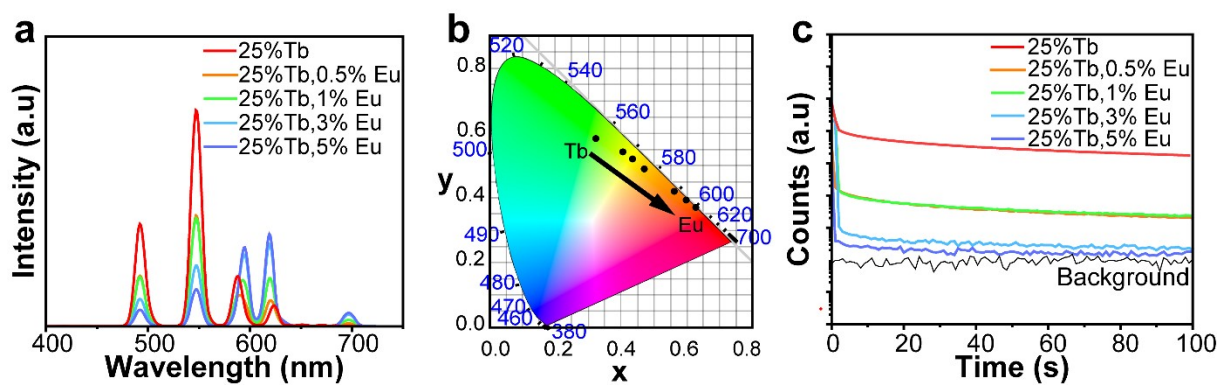


Figure S9. Tunable spectra of NaYF₄ co-doped with Tb³⁺ and Eu³⁺. Controlling for the constant Tb³⁺ content, the Eu³⁺ concentration-dependent of (a) X-ray luminescence spectra, (b) corresponding Commission Internationale de l'Eclairage (CIE) chromaticity diagram, and (c) afterglow spectra.

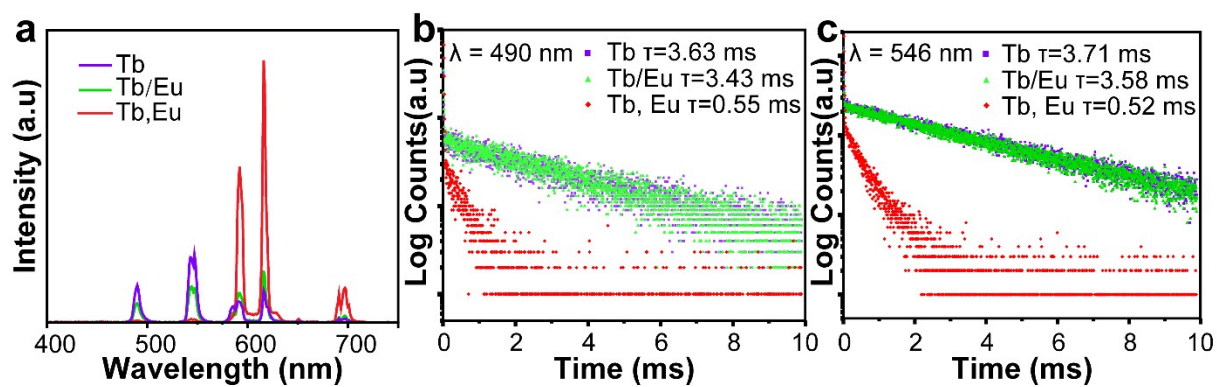


Figure S10. (a) Fluorescence spectra of NaYF₄:Tb³⁺(25 mol%), NaYF₄:Tb³⁺(25 mol%)/NaYF₄:Eu³⁺(15 mol%), and NaYF₄:Tb³⁺, Eu³⁺(25, 0.5 mol%) under 379 nm excitation. Fluorescence lifetime spectra at 379 nm excitation with detection wavelengths of (b) 490 nm and (c) 546 nm.

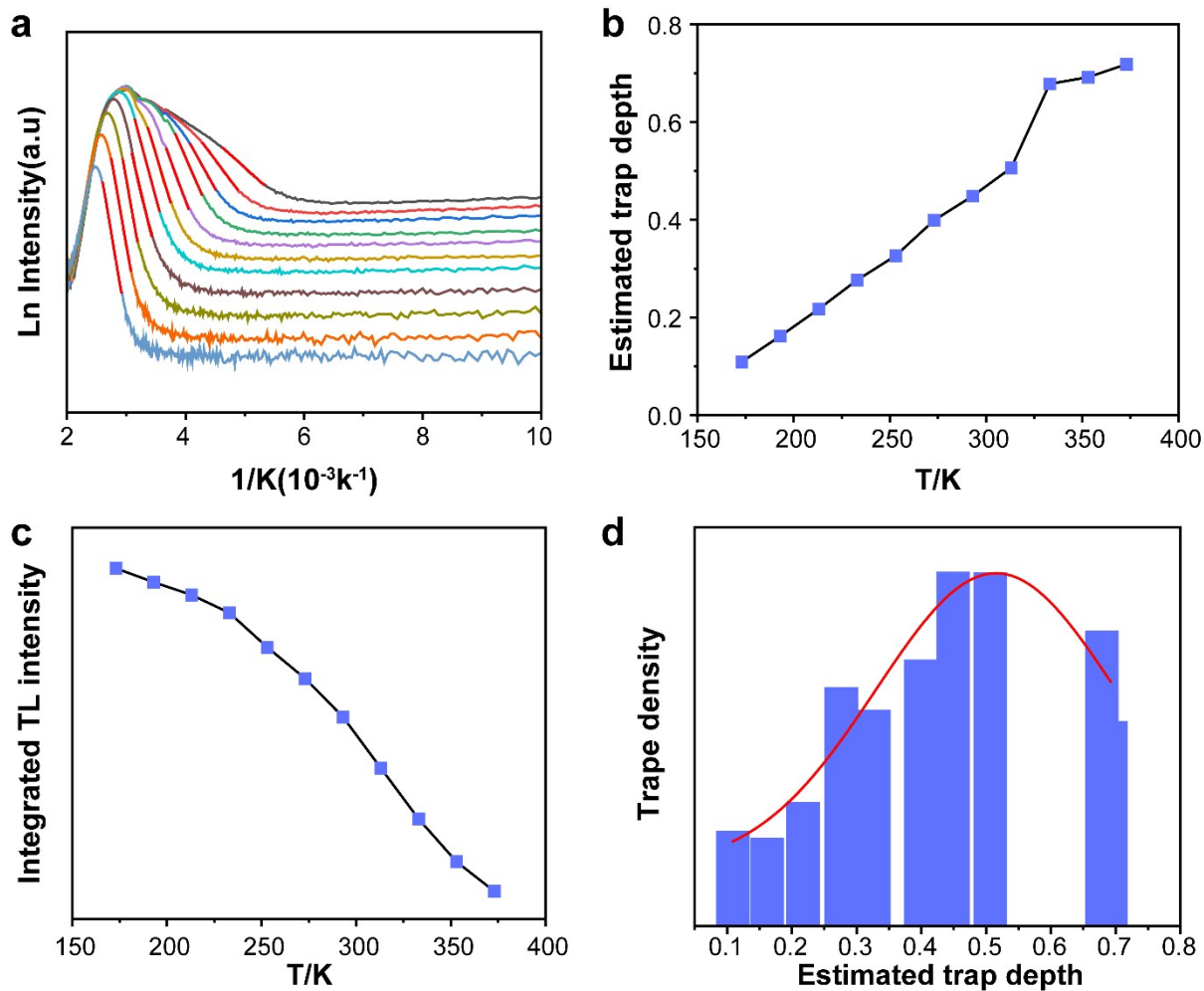


Figure S11. Thermoluminescence curves of NaYF₄:Tb³⁺(25 mol%) microrods tested in the temperature range of 173-373 K. The initial rise method (a) was used to calculate (b) the depth of the defect energy level for each temperature and (c) the integrated area of the peaks of the pyroelectric curve at different excitation temperatures based on the fitted slopes of the thermoluminescence curves. (d) Energy level density for each defect energy level.

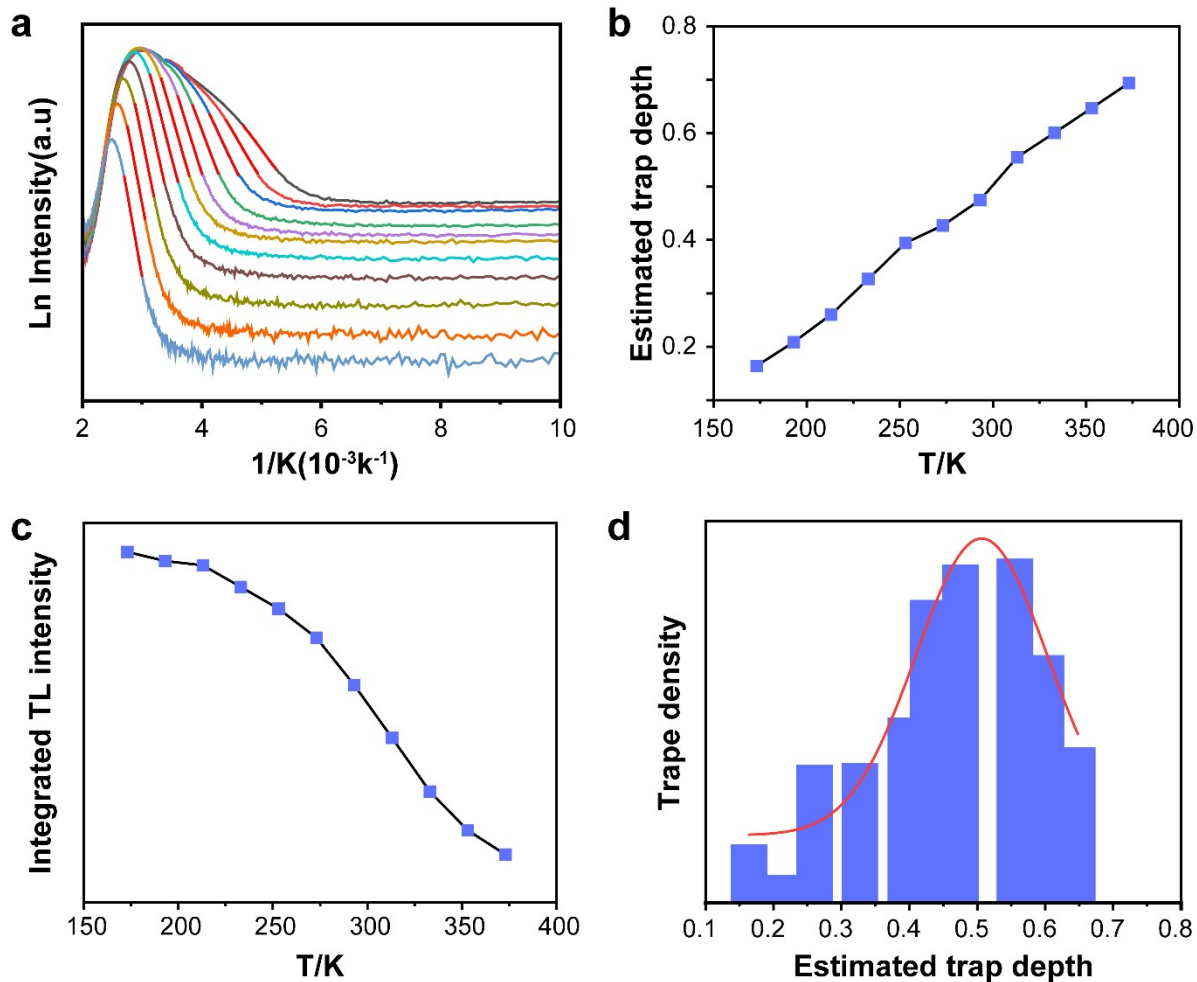


Figure S12. Thermoluminescence curves of NaYF₄:Tb³⁺(25 mol%)/NaYF₄:Eu³⁺(15 mol%) microrods tested in the temperature range of 173-373 K. The initial rise method (a) was used to calculate (b) the depth of the defect energy level for each temperature and (c) the integrated area of the peaks of the pyroelectric curve at different excitation temperatures based on the fitted slopes of the thermoluminescence curves. (d) Energy level density for each defect energy level.